A transferable force field for CdS-CdSe-PbS-PbSe solid systems

Zhaochuan Fan,[1] Rik S. Koster,[2] Shuaiwei Wang,[3] Changming Fang,[2] Anil O. Yalcin,[4] Frans D. Tichelaar,[4] Henny W. Zandbergen,[4] Marijn A. van Huis,[2] and Thijs J. H. Vlugt[1,a)]
[1]*Process and Energy Department, Delft University of Technology, Leeghwaterstraat 39, 2628 CB Delft, The Netherlands*
[2]*Debye Institute for Nanomaterials Science and Center for Extreme Matter and Emergent Phenomena, Utrecht University, Princetonplein 5, 3584 CC Utrecht, The Netherlands*
[3]*Institute of Nanostructured Functional Materials, Huanghe Science and Technology College, Zhengzhou, Henan 450006, China*
[4]*Kavli Institute of Nanoscience, Delft University of Technology, Lorentzweg 1, 2628 CJ Delft, The Netherlands*

(Received 8 September 2014; accepted 1 December 2014; published online 29 December 2014)

A transferable force field for the PbSe-CdSe solid system using the partially charged rigid ion model has been successfully developed and was used to study the cation exchange in PbSe-CdSe heteronanocrystals [A. O. Yalcin *et al.*, "Atomic resolution monitoring of cation exchange in CdSe-PbSe heteronanocrystals during epitaxial solid-solid-vapor growth," Nano Lett. **14**, 3661–3667 (2014)]. In this work, we extend this force field by including another two important binary semiconductors, PbS and CdS, and provide detailed information on the validation of this force field. The parameterization combines Bader charge analysis, empirical fitting, and *ab initio* energy surface fitting. When compared with experimental data and density functional theory calculations, it is shown that a wide range of physical properties of bulk PbS, PbSe, CdS, CdSe, and their mixed phases can be accurately reproduced using this force field. The choice of functional forms and parameterization strategy is demonstrated to be rational and effective. This transferable force field can be used in various studies on II-VI and IV-VI semiconductor materials consisting of CdS, CdSe, PbS, and PbSe. Here, we demonstrate the applicability of the force field model by molecular dynamics simulations whereby transformations are initiated by cation exchange. [http://dx.doi.org/10.1063/1.4904545]

I. INTRODUCTION

Transition metal monochalcogenides with the formula ME (M is a transition metal, E = S, Se, or Te) are key materials in the development of nanoscience and nanotechnology.[1–4] Within this class of materials, cadmium chalcogenides (CdE) and lead chalcogenides (PbE) are abundantly used because of their intriguing physical properties. CdE are wide-bandgap II-VI semiconductors with four-fold coordinated wurtzite (WZ) or zinc blende (ZB) crystalline structures.[5] CdE nanostructures show quantum confinement so that the effective band gap depends on the crystalline size.[6] PbE belong to IV-VI semiconductors forming a six-fold rocksalt (RS) crystalline structure,[7] which are important thermoelectric materials with a low thermal conductivity and high thermoelectric figures of merit.[8,9] CdE and PbE nanocrystals (NCs) can be synthesized in diverse morphologies, e.g., spheres, cubes, rods, tetrahedrons, truncated octahedron, and hexagonal disks.[1,10–15] These NCs can also be used as seeds in the seed growth (SG) process to obtain heteronanocrystals (HNCs) such as core-shell and core-multishell structures, tetrapods and octapods, and nanodumbbells.[16–19] Recently, oriented attachment (OA)[20] and ion exchange (IE)[21,22] have been shown to be very powerful tools in the synthesis and design of nanostructures. In OA, NCs are used as building blocks and are assembled in different patterns depending on the preferred attachments of particular facets.[20,23] In the IE process, either the cations or anions in a nanostructure are partially or completely replaced by a substitutional ion from a solution or vapor.[21,22] OA and IE can be independently used[24–31] or combined[32] to synthesize nanostructures such as nanowires, nanorod couples, dimers, thin films, and 2-D superlattices. They are promising techniques in the design and application of nanomaterials and nanodevices.

To theoretically study bulk crystalline materials, first principles density functional theory (DFT) calculations using three-dimensional periodic boundary conditions provide reliable and accurate results within affordable computational requirements.[30,33–38] However, to simulate NCs containing more than a few thousands of atoms, DFT calculations are no longer possible because of the huge computational demands. Instead, classical molecular simulations techniques such as molecular dynamics (MD) or Monte Carlo (MC) using classical force fields are more commonly used to deal with large systems.[30,39–41] Deriving accurate force fields using appropriate functional forms is an essential prerequisite for performing reliable and accurate classical MD and MC simulations.

There is limited number of force field models developed for cadmium chalcogenides. Wright and Gale[42] proposed a transferable shell model (SM) for both ZnS and CdS. The SM has a long history of success in modeling ionic materials.[43] In such a model, an ion is presented by a massive and positively

a)Electronic mail: t.j.h.vlugt@tudelft.nl

charged core and a massless and negatively charged shell, and a "spring" is used to connect the core and shell, thus the SM is able to describe ionic polarizability. The SM developed by Wright and Gale[42] is able to accurately reproduce several physical properties for ZnS but has a poor performance for CdS. Moreover, there are three limitations in this SM: (1) most transition metal chalcogenides are partially ionic and partially covalent,[44] but full integer charges, ±2 *e* were still used in this model. The use of integer charges in force fields of ionic solid materials helps their transferability and enables modelling of the energy and local structure of defects in the materials.[45–48] However, there is also evidence that force fields developed for ionic solids using partial charges[33,39,49] have superior performance to those using integer charges[42,50,51] for reproducing physical properties such as lattice parameters, elastic constants, and phase stabilities; (2) Three-body and four-body interatomic interaction potentials were used in this SM to stabilize the tetrahedrally coordinated structure of CdS and ZnS. Three-body interatomic interaction potentials are often used to describe the directional feature of the covalent bonds. However the presently used functional forms of these angle dependent potentials[42,52] are often pointed to the materials' stable phases with a particular bond angle (e.g., 104.7° for tetrahedral coordination structures), thus the stabilities for other structures with different bond angles (e.g., 90° and 180° for octahedral coordination structures) are significantly underestimated. (3) One third of the total atoms are extra "shell" atoms which decreases the computational efficiency. Other interaction models which do not include charges and attempt to incorporate Coulomb interactions into effective two-body or many-body interactions. Two examples thereof are a transferable Stillinger-Weber (SW) potential developed for the Zn-Cd-Hg-S-Se-Te system[52] and a analytical bond order potential (ABOP) for Cd-Zn-Te systems.[53] These potentials cover several elements and can accurately reproduce the lattice parameters, elastic properties, and cohesive energies for II-VI binary compounds in the four-fold WZ or ZB structures. However, both the SW potential[52] and the ABOP[53] models failed to accurately reproduce the relative stabilities between the six-fold RS phase and the four-fold WZ and ZB phases. Therefore, the description of the pressure-induced ZB-to-RS or WZ-to-RS phase transitions in II-VI binary compounds using these potential models could be questionable. A simple but effective partially charged rigid ion model (PCRIM)[54] was first used to develop a pair potential for CdSe by Rabani,[55] and the model was extended to CdS and ZnS by Grünwald *et al.*[39] In this model, effective charges of ±1.18 *e* were set for cations and anions, and Lennard-Jones (LJ) potentials were used to describe the short-range interactions (this model will be referred as the LJ model below).[39,55] Unlike the SM, SW potentials, and the ABOP model mentioned above[42,52,53] which are only valid to describe the four-fold WZ and ZB phases, this LJ model captured the energy features for three phases, WZ, ZB, and RS.[39,55] Therefore, it has been frequently used in simulation studies of phase transitions.[40,56–58] One minor flaw in this LJ model is that the parameterization was over-constrained: both the cation-cation and anion-anion short-range interatomic interactions were included and the remaining parameters in the cross terms (cation-anion, S-Se, and Zn-Cd short-range interatomic interactions) were obtained by the Lorentz-Berthelot mixing rules. Using too many constrains in the fitting procedures decreases the degrees of the freedom, thus may lead to less accurate results. For example, the calculated bulk moduli of CdS and CdSe by this LJ model were smaller than the experimental data, and physical properties of ZnSe cannot be accurately described by this LJ model.[39] There are even fewer force fields published for lead chalcogenides. Schapotschnikow *et al.*[59] derived a pair potential model for PbSe within the same LJ model approach and used it in the atomistic simulations of the morphological transformations and fusion of PbSe NCs. In this LJ model for PbSe, the effective charges for Pb and Se ions are ±1.29 *e*, and the parameters that describe the Se-Se short-range interactions in PbSe are very different from that in the LJ model for CdSe.[55] Therefore, to describe the PbSe-CdSe ternary system, this PbSe LJ model[59] cannot be easily combined with the CdSe LJ model.[55] The PCRIM has also been applied to develop force fields for PbTe.[34,60] To our best knowledge, no force field has yet been published for PbS.

When deriving force fields for ionic solid materials, it is important to note the following: (1) for half-ionic-half-covalent materials, the use of partial (effective) charges has a considerable advantage over using full integer charges.[33] (2) Although three-body and many-body interactions may exist in the systems, including them in a force field model should be applied with caution. In many cases, force fields consisting of only pair potentials can already describe a wide range of polymorphs for materials with considerably good accuracy,[33,39,55,59] but those including many-body potentials can often be applied to fewer phases.[34,42,52] (3) Force fields developed by following a conventional fitting procedure whereby the training sets merely include available experimental data cannot satisfy the increasing needs of high accuracy and wide utilizable range.[61] (Training sets are the sets of data used to fit the potential to, in contrast to the validation sets that are not included in the fit, and which serve to test the performance of the force field.) DFT and *ab-initio*-MD data are commonly included in the training sets to develop "nearly prefect" force fields to describe not only crystal structures, elastic, and vibration properties but also properties of high-pressure, metastable, liquid, and gas phases, and of different surfaces and interfaces.[33,34,47,53,59] On the other hand, a classical force field can never be prefect and one should be aware of the limitations of a force field.

Very recently, we have developed a transferable PCRIM for the PbSe-CdSe ternary system and used it in a MD study of cation exchange in PbSe-CdSe HNCs.[30] In this model, the values of the effective charges were determined by a Bader analysis.[62] The short-range interatomic interaction potentials were parameterized to reproduce the lattice parameters, elastic properties, and relative stability for CdSe and PbSe polymorphs. In particular, we included the relative stabilities of stable WZ and ZB, high-pressure RS and CsCl, and metastable honeycomb (HC) phases from DFT calculations in the training set to ensure an accurate description of the possible structural transitions.[30] In this work, we extend the transferable force field to cover the CdS-CdSe-PbS-PbSe systems, four binary compounds, and their mixed phases. DFT calculations for the

four II-VI and IV-VI binary compounds and a board range of validation tests for the force field are also provided in detail.

The paper is structured as follows. In Sec. II, we introduce the methods used in the DFT calculations, fitting procedures, and MD simulations. Different crystal structures of CdX (X = S or Se) and PbX crystals are also introduced in this section. In Sec. III, the lattice parameters, elastic properties, relative stability, transition pressures, and phonon dispersion relations of MX bulk materials are calculated by this force field and are compared to the values calculated by other force fields, the DFT calculations, and the experimental data. In Sec. IV, we use the transferable force field to calculate several physical properties of four ternary mixed phases. Different behavior is found between the MS_xSe_{1-x} and $Cd_xPb_{1-x}X$ systems while changing the fraction x. In Sec. V, to test the suitability of this force field for simulating the behaviors of nanostructures, we calculate the surface energy of several different non-polar surfaces of WZ-CdX and RS-PbX and compare them with DFT calculations. In Sec. VI, we summarize the results.

II. METHODS

A. Density functional theory calculations

First principles DFT calculations were employed to calculate the crystal structures and relative stabilities of CdS, CdSe, PbS, and PbSe polymorphs and their mixed phases, as well as the surface energies for several different non-polar surfaces in WZ-CdX and RS-PbX. For each material, calculations were performed for five polymorphs: WZ, RS, ZB, HC, and CsCl (Figures 1(a)-1(e)). By a full structural optimization, WZ-PbX will automatically transfer into a five-fold HC structure, which indicates that the WZ phase is unstable for PbS and PbSe. A Bader charge analysis[62] was carried out to determine the effective charges on the atoms for each polymorph. For the details of these DFT calculations, we refer to our previous works.[30,33] The results of the Bader charges of the cations are listed in Table I. Differences between the Bader charges of different materials and different structures are small. These similar Bader charges enable us to develop a transferable force field with a uniform absolute value of effective charge for all four materials. The effective charges were fixed at ±0.8 *e* for all cations and anions as in our previous work.[30]

To provide DFT data of the mixed phases for the fitting procedure, four quasi-mixed phases (QMPs) were constructed by replacing half of the total anions in a unit cell (S and Se) with the other type (Se or S). Thus the formulas of these QMPs are Cd_2SSe and Pb_2SSe. Due to the relatively small unit cell used, rather than being randomly distributed, the two different anions are arranged in alternate layers in the QMPs when 3-D periodic boundary conditions applied. We labeled these QMPs as WZ', RS', ZB', and HC' to correlate them with their original crystal structures and also to mark the reduced symmetry of

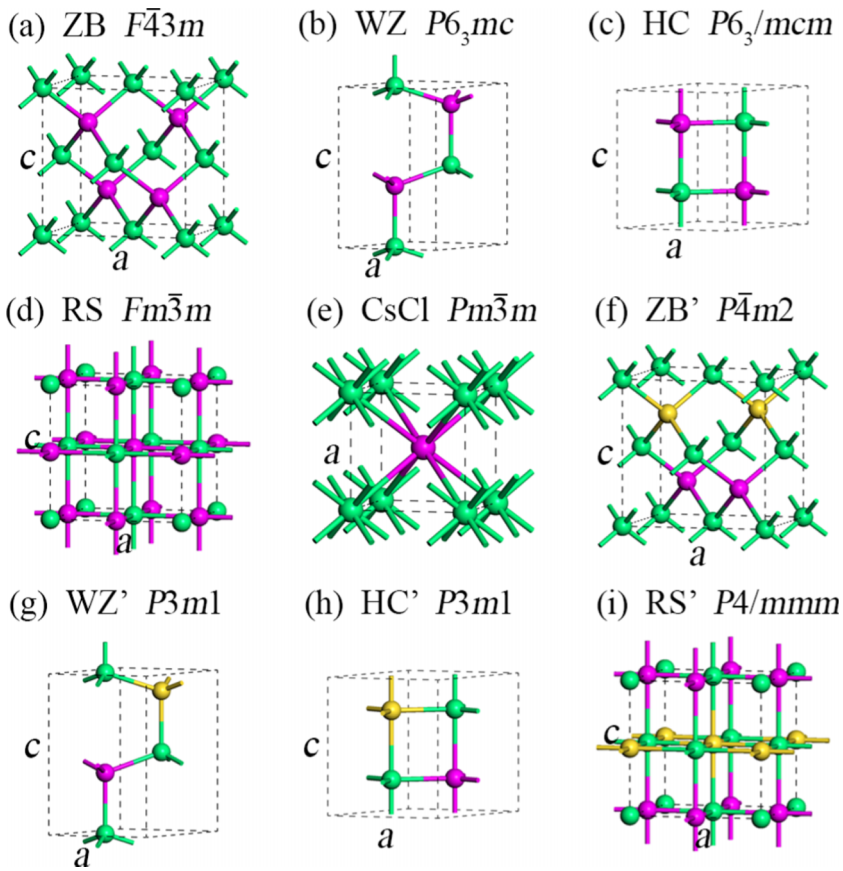

FIG. 1. Unit cells for binary compounds ((a)-(e)) and for QMPs ((f)-(i)). (a) ZB, (b) WZ, (c) HC, (d) RS, (e) CsCl, (f) ZB', (g) WZ', (h) HC', and (i) RS'. The space groups are listed for each structures. The green spheres represent one type of cations (Cd or Pb); yellow and purple spheres represent two different anions (S and Se).

TABLE I. DFT-calculated Bader charges of cations in CdS, CdSe, PbS, and PbSe polymorphs (details in main text). All charges are in e.

	CsCl	RS	ZB	WZ	HC
CdS	0.847	0.810	0.852	0.867	0.843
CdSe	0.712	0.825	0.725	0.711	0.750
PbS	0.929	1.001	0.913	. . .	0.933
PbSe	0.813	0.812	0.804	. . .	0.781

these QMPs with a prime symbol. Schematic representations of these QMPs are shown in Figures 1(f)-1(i) together with their space groups. Note that because of the reduced symmetry in these QMPs, the internal coordinations in these QMPs may differ from those in their correlated crystal structures, and for ZB' and RS', lattice parameter a is not necessarily equal to c. Full structural optimization were carried out for WZ'-, ZB'-, and RS'-Cd_2SSe and HC'-, ZB'-, and RS'-Pb_2SSe. The basic set-up of DFT calculations for each QMP is the same as that for its correlated crystal structure.

B. Fitting methodology

The functional format of the interaction potentials for CdS and PbS were kept the same as those for CdSe and PbSe.[30] It only contains Coulomb interactions and short-range two-body interactions[30]

$$U_{ij} = \frac{q_i q_j}{r_{ij}} + Ae^{-r_{ij}/\rho} - \frac{C_6}{r_{ij}^6}. \quad (1)$$

The first term describes the long-range Coulomb interactions. The second and the third terms are the Buckingham potential that describes the repulsive and dipole-dipole interactions. A, ρ, and C_6 are parameters to be obtained by fitting. The short-range cation-cation interactions (the Buckingham potential) are ignored.

Both a conventional and relaxed fitting procedure[61] were used to obtain the parameters. Empirical fitting based on experimental data and relaxed *ab-initio* energy surface fitting[30,33] based on DFT data were combined to obtain all parameters. All 18 parameters in the Buckingham potentials were relaxed simultaneously and obtained by fitting to the experimental data, including the lattice parameters and elastic constants of RS-PbX, WZ-, and ZB-CdX measured at room temperature, as well as the DFT data, including the lattice parameters and relative stabilities of RS-, ZB-, CsCl-, and HC-PbX and WZ-, ZB-, RS-, and HC-CdX. For DFT-GGA calculations are generally known to systemically show larger lattice parameters in comparison to experimental data. The lattice parameters obtained by our DFT-GGA calculations were normalized by rescaling their volumes.[30,33] All calculations in the fitting procedures were carried out by GULP.[63] A cut-off radius of 12 Å was set for the short-range Buckingham potentials. The Ewald summation method[64,65] was used to calculate the electrostatic interactions. Further details about the fitting procedures can be found elsewhere.[30]

To complete the parameter set, the parameters of the short-range S-Se Buckingham potential are also required. These parameters were obtained by fitting the DFT data of the lattice parameters, internal coordinations, and relative stabilities of the QMPs (WZ'-, ZB'-, and RS'-Cd_2SSe; and RS'-, ZB'-, and HC'-Pb_2SSe). The lattice parameters of the QMPs from the DFT-GGA calculations were also rescaled[30,33] for fitting. During fitting, all previously determined parameters remained unchanged, only the three parameters A, ρ, and C_6 in the S-Se Buckingham potential were relaxed. The complete parameter set of the transferable force field for CdS-CdSe-PbS-PbSe system is listed in Table II.

TABLE II. The complete set of parameters of the transferable force field for CdS, CdSe, PbS, PbSe, and their mixed phases (see Eq. (1)). Parameters A, ρ, and C are in eV, Å, and eV·Å^6, respectively. The short-range interactions between cations are ignored. The effective ion charges q are ±0.8 e.

Interaction	A	ρ	C
Cd-S	1.26×10^9	0.107	53.5
Cd-Se	2.64×10^9	0.108	64.4
Pb-S	3.05×10^6	0.173	154
Pb-Se	4.88×10^6	0.173	211
S-S	4.68×10^3	0.374	120
Se-Se	5.20×10^3	0.384	127
S-Se	5.44×10^3	0.376	122

C. Molecular dynamics simulations

MD simulations were used to compute several properties of the CdX and PbX and their mixed phase at finite temperatures. For bulk materials, periodic matrices containing about 4000 atoms were constructed for WZ- and ZB-CdX and RS-PbX based on the experimental lattice parameters. In the MD simulations, the equations of motion were integrated using the velocity Verlet algorithm with a time step of 1 fs. At $T = 300$ K and $p = 0$ GPa, each MD simulation of 0.5 ns was performed in the isobaric-isothermal (NpT) ensemble. The first 0.1 ns was used for equilibration whereby the velocities were rescaled to the target temperature. This MD time is long enough to equilibrate the systems. The temperature and the pressure were controlled by a standard Nosé-Hoover thermostat and barostat.[66]

III. PHYSICAL PROPERTIES OF CdS, CdSe, PbS, AND PbSe BINARY COMPOUNDS

We first test our transferable force field by reproducing the geometrical structures and elastic properties of CdX and PbX. For the lattice parameters, we considered five structures (WZ, ZB, RS, HC, and CsCl) for CdX and four structures (RS, ZB, HC, and CsCl) for PbX. For the elastic constants and bulk moduli, we only considered the most stable phases for CdX (WZ and ZB) and PbX (RS). Reliable experimental data are only partially available for the lattice parameters, elastic constants, and bulk moduli of these binary compounds in their stable and high-pressure phases. Lattice parameters for the other phases can only be compared with DFT calculations. In addition, MD simulations were performed for the stable phases for each material to obtain the lattice parameters at finite temperature (300 K). The results are listed in

TABLE III. Lattice parameters of CdS, CdSe, PbS, and PbSe polymorphs calculated by lattice statics and MD simulations using the present force field, compared with experimental and DFT data and the results calculated by the LJ models of Refs. 39 and 59. Lattice parameters a and c are in Å; u is the internal coordinate. The values in parentheses are MD results at 300 K; the values in square brackets are normalized lattice parameters from DFT calculations; the values in bold are data used for the fit of the force field parameters.

	CsCl	RS	ZB	WZ			HC	
	a	a	a	a	c	u	a	c
CdS								
Expt.	. . .	5.32 (4.3 GPa)[a]	5.83[b]	**4.14**[b]	**6.72**[b]	**0.378**[b]	. . .	. . .
PCRIM, this work	3.59	5.39	5.81 (5.86)	4.13 (4.17)	6.63 (6.69)	0.379	4.38	5.54
LJ model[c]	3.53	5.43	5.83	4.16	6.59	0.384	4.43	5.52
DFT, this work	3.42 [3.36]	5.51 [**5.41**]	5.94 [**5.83**]	4.21	6.85	0.377	4.45 [**4.37**]	5.82 [**5.72**]
CdSe								
Expt.	. . .	5.54 (4.8 GPa)[d]	6.08[b]	**4.30**[b]	**7.01**[b]	**0.376**[b]	. . .	. . .
PCRIM, this work	3.77	5.63	6.08 (6.13)	4.32 (4.36)	6.94 (7.00)	0.379	4.57	5.63
LJ model[c]	3.75	5.74	6.14	4.38	6.96	0.383	4.64	5.94
DFT, this work	3.56 [3.49]	5.75 [**5.63**]	6.21 [**6.08**]	4.39	7.17	0.377	4.66 [**4.56**]	6.07 [**5.94**]
PbS								
Expt.	3.29 (25 GPa)[e]	**5.94**[f]	. . .	. . .	. . .	. . .	. . .	. . .
PCRIM, this work	3.62	5.94 (5.99)	6.67	. . .	. . .	. . .	5.06	5.91
DFT, this work	3.64 [**3.61**]	6.00	6.64 [**6.58**]	. . .	. . .	. . .	5.03 [**4.98**]	6.01 [**5.95**]
PbSe								
Expt.	3.38 (30 GPa)[e]	**6.12**[f]	. . .	. . .	. . .	. . .	. . .	. . .
PCRIM, this work	3.71	6.09 (6.13)	6.84	. . .	. . .	. . .	5.18	6.05
LJ model[g]	3.66	6.05	6.77	. . .	. . .	. . .	5.14	6.01
DFT, this work	3.77 [**3.72**]	6.21	6.89 [**6.80**]	. . .	. . .	. . .	5.21 [**5.14**]	6.23 [**6.15**]

[a]Reference 67.
[b]Reference 5.
[c]Calculated using the LJ model reported in Ref. 39.
[d]Reference 68.
[e]Reference 69.
[f]Reference 7.
[g]Calculated using the LJ model reported in Ref. 59.

TABLE IV. Elastic constants and bulk moduli of WZ-, ZB-CdX, and RS-PbX calculated using the present force field and the LJ models of Refs. 39 and 59, together with experimental data. The elastic constant c_{ij} and bulk modulus B are in GPa. The values in bold are data used for the fit of the force field parameters.

	c_{11}	c_{12}	c_{13}	c_{33}	c_{44}	c_{66}	B
WZ-CdS							
Expt.[a]	**86.5**	**54.0**	**47.3**	**94.4**	**15.0**	**16.3**	**62.7**
PCRIM, this work	85.3	56.2	48.4	85.4	14.6	14.5	62.3
LJ model[b]	79.4	47.9	41.8	74.8	17.6	15.7	55.0
ZB-CdS							
Expt.[a]	**77.0**	**53.9**	...	...	**23.6**	...	**61.6**
PCRIM, this work	72.4	57.2	...	...	24.2	...	62.3
LJ model[b]	65.0	50.0	...	...	27.7	...	55.0
WZ-CdSe							
Expt.[a]	**74.1**	**45.2**	**39.0**	**84.3**	**13.4**	**14.5**	**53.1**
PCRIM, this work	72.4	47.9	41.4	72.5	12.3	12.2	53.1
LJ model[b]	65.9	38.0	32.9	64.4	15.2	14.0	44.8
ZB-CdSe							
Expt.[a]	**66.7**	**46.3**	...	...	**22.3**	...	**53.1**
PCRIM, this work	61.6	48.8	...	...	20.3	...	53.1
LJ model[b]	53.8	40.2	...	...	24.2	...	44.7
RS-PbS							
Expt.[c]	**126.0**	**16.0**	...	...	**17.0**	...	**49.9**
PCRIM, this work	127.0	16.3	...	...	16.3	...	53.2
RS-PbSe							
Expt.[c]	**123.7**	**19.3**	...	...	**15.9**	...	**54.1**
PCRIM, this work	129.9	16.5	...	...	16.5	...	54.3
LJ model[d]	125.0	19.1	...	...	19.1	...	54.4

[a]Reference 5.
[b]Calculated using the LJ model reported in Ref. 39.
[c]Reference 7.
[d]Calculated using the LJ model reported in Ref. 59.

Tables III and IV for lattice parameters and elastic properties, respectively, together with available experimental data, DFT calculations, and the results calculated using the LJ models.[39,55,59] It should be clarified that most of these physical properties were used in the fitting procedure as training sets, therefore our potential set was expected to accurately reproduce these properties. As is shown in Tables III and IV, this new force field is able to accurately reproduce all properties concerned for all four binary compounds. Compared to other models,[39,55,59] our force field model shows equivalent or higher accuracy when reproducing lattice parameters and elastic properties. Note that we repeated the calculations using the previous LJ models for CdS,[39] CdSe,[55] and PbSe.[59] The results were slightly different from the original values reported.[39,55,59]

The cohesive energy, defined as the energy required for separating a solid or liquid into isolated free atoms, is often used to describe the energy features of condensed materials and to compare the energies of a material between different phases. Cohesive energies of solids can be either measured by experiments or calculated by DFT. The cohesive energies of WZ-CdX and RS-PbX calculated by DFT-GGA are listed in Table V. The DFT-calculated cohesive energies of CdS and CdSe are 6.603 and 5.414 eV/f.u., respectively, which are slightly larger than the experimentally measured values[70] of 5.71 and 4.93 eV/f.u. for CdS and CdSe, respectively. The cohesive energies by DFT calculations are 8.640 and 8.065 eV/f.u. for PbS and PbSe, respectively. For PbX, there is no available experimental data for comparison. These DFT-calculated cohesive energy values were not included in the training set for fitting, because the PCRIM was chosen to describe the interatomic interactions whereby the ions remain charged while being pulled apart from each other.[33] Therefore, force field models with fixed charges are only applicable to calculating lattice energies (the energy required for separating a solid into a gas of its ions). The lattice energies calculated with the present force field are −6.320, −6.027, −6.034, and −6.079 eV/f.u for WZ-CdS, WZ-CdSe, RS-PbS, and RS-PbSe, respectively. For a more detail discussion on the difference between the lattice energy and the cohesive energy, the reader is referred to Refs. 33 and 45.

Compared to reproducing the absolute energies (cohesive energy or lattice energy), accurately reproducing the relative stability (energies) of different phases of a material is more important for a force field to accurately simulate solid-solid phase transitions.[33] The relative stability of polymorphs was included in the training set, thus assuring accuracy in describing the related solid-solid phase transitions.[33] The calculated relative stabilities are also listed in Table V, in comparison with the data calculated with the LJ models[39,55,59] and by DFT-GGA. According to our DFT-GGA results, CdS and CdSe have very similar relations of the phase stabilities. The order of their polymorphic stabilities is $E_{WZ} \sim E_{ZB} < E_{HC} < E_{RS} < E_{CsCl}$. Here, E can either be the opposite number of cohesive energy or the total energy. Note that our DFT-GGA calculations

TABLE V. Relative energy differences of CdS, CdSe, PbS, and PbSe polymorphs calculated using the present force field and the LJ models of Refs. 39 and 59, in comparison with DFT data. The number 0 indicates the most stable phase among the polymorphs. The values in parentheses are the cohesive energies calculated by DFT or the absolute values of the lattice energies calculated with the force fields. The values in bold are data used for the fit of the force field parameters. The energy differences, cohesive energies, and lattice energies are reported in eV/f.u.

	CsCl	RS	ZB	WZ	HC
CdS					
DFT, this work	1.278	**0.268**	**0.002**	**0** (6.063)	**0.180**
PCRIM, this work	1.341	0.297	0.015	0 (6.320)	0.149
LJ model[a]	1.358	0.095	0.030	0 (12.095)	0.066
CdSe					
DFT, this work	1.200	**0.292**	**0**	**0.002** (5.414)	**0.210**
PCRIM, this work	1.290	0.291	0.014	0 (6.027)	0.149
LJ model[a]	1.396	0.148	0.027	0 (11.486)	0.082
PbS					
DFT, this work	**0.508**	**0** (8.640)	**0.380**	. . .	**0.316**
PCRIM, this work	0.467	0 (6.034)	0.360	. . .	0.373
PbSe					
DFT, this work	**0.478**	**0** (8.065)	**0.374**	. . .	**0.320**
PCRIM, this work	0.528	0 (6.079)	0.381	. . .	0.397
LJ model[b]	0.428	0 (12.922)	0.464	. . .	0.423

[a]Calculated using the LJ model reported in Ref. 39.
[b]Calculated using the LJ model reported in Ref. 59.

predicted a higher stability of the HC phase than the RS phase for CdSe at zero temperature and zero pressure conditions, in contrast to previous DFT calculations whereby the local density approximation (LDA) was used.[35] In general, both of our new transferable PCRIM and the previous LJ model[39,55] can correctly reproduce the order of the stabilities for CdX. We first discuss the relative stabilities of the WZ, HC, and RS phases, which are involved in the extensively studied pressure-induced WZ-to-RS phase transition.[36,37,56–58,71–73] Figure 2 shows the enthalpies (H) of CdX with the WZ and RS structures as a function of hydrostatic pressure at 0 K. The points where $H_{WZ} = H_{RS}$ are 4.8 and 4.1 GPa for CdS and CdSe, respectively.

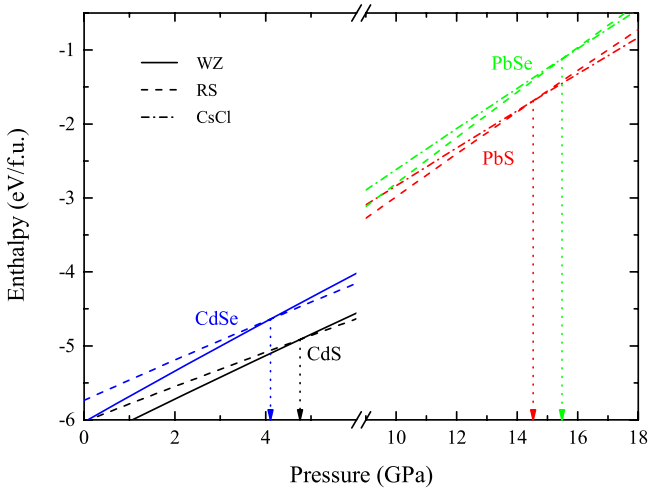

FIG. 2. Calculated enthalpies (H) as a function of hydrostatic pressure for CdS (black lines), CdSe (blue lines), PbS (red lines), and PbSe (green lines) in the WZ (solid lines), RS (dashed lines), and CsCl (dashed-dotted line) structures. The vertical arrow indicates the pressure where $H_{WZ} = H_{RS}$ or $H_{RS} = H_{CsCl}$.

These results are in good agreement with the recently reported experimental measurements of the transition pressures for CdS (3.0 ~ 4.3 GPa)[67] and CdSe (3.0 ~ 4.8 GPa).[68] The LJ model[39,55] for CdS and CdSe shows smaller values of ΔE_{RS-WZ} and ΔE_{HC-WZ} compared to our force field model and DFT-GGA calculations, thus yielding slightly lower transition pressures.[39] Both the present model and the LJ model[39,55] show similar ratios of $\Delta E_{HC-WZ}/\Delta E_{RS-WZ} \sim 0.5$ which is smaller than the DFT results of ~0.7. This deviation may contribute to a slightly biased preference of the HC phase as an intermediate phase in the route of the WZ-to-RS phase transition when applying these models.[56,57,74] To the best of our knowledge, the classical force field model presented in this work provides the most accurate description of the pressure-induced WZ-to-RS phase transition for CdS and CdSe.

Another issue is the relative stability of the WZ and ZB structures in CdX. In II-VI group semiconductors, some materials form the WZ structure in nature (e.g., ZnO, CdS, and CdSe) and some form the ZB structure (e.g., CdTe, ZnS, ZnSe, and ZnTe). The relative stability of WZ and ZB is similar (energy difference less than a few meV/atom), especially for CdS and CdSe which have almost the same stability or energy of the WZ and ZB polymorphs at zero temperature zero pressure conditions based on DFT calculations. Calculated using a force field for tetrahedrally coordinated materials that only contain Coulomb interactions and two-body potentials, the WZ phase is always more stable than the ZB phase.[33,39,47,55,75] This is naturally true for ZnO,[33,47] but not for other II-VI semiconductors. To correct this issue, three-body and even four-body interactions were proposed to be added in force field models for CdS and ZnS.[42,76] This restricts the utilizable range of the force field to only the four-fold WZ or ZB structures. The functions used for the three-body interactions resulted into a unique preferred bond angle of 109.5°, which

led to an artificially low stability of other non-tetrahedrally coordinated phases (e.g., the six-fold RS phase). The same problem also exists in the SW potential,[52] which yields exactly equal stability for WZ and ZB but significantly underestimated the relative stability of the high-pressure RS phase ($\Delta E^{\mathrm{SW-CdS}}_{\mathrm{RS-WZ}}$ = 1576 meV/f.u. and $\Delta E^{\mathrm{SW-CdSe}}_{\mathrm{RS-WZ}}$ = 1168 meV/f.u.). Calculated using our new force field model, the relative stabilities of ZB with respect to WZ are 15 and 13 meV/f.u. for CdS and CdSe, respectively, while those calculated by the LJ model[39,55] are 30 and 27 meV/f.u. for CdS and CdSe, respectively. Both numbers are higher than that computed from DFT ($\Delta E^{\mathrm{CdS}}_{\mathrm{ZB-WZ}}$ = 2 meV/f.u. and $\Delta E^{\mathrm{CdSe}}_{\mathrm{ZB-WZ}}$ = −2 meV/f.u.). This deviation in our force field or the LJ model[39,55] can be neglected since the energy differences are less than the thermal energy, k_BT.

The pressure-induced RS-to-CsCl phase transitions in PbX is more complicated: several intermediate states may coexist and the mechanism is still under debate.[69,77,78] For PbX, we mainly focus on the phase stability of RS, CsCl, ZB, and HC which are the stable phase, the high-pressure phase, and two metastable phases at negative pressure, respectively. The relative energy of the CsCl, ZB, and HC phases with respect to the stable RS phase for PbX calculated by DFT is in range of 0.3 ~ 0.5 eV/f.u.. Both our new potential set for PbX and the LJ model for PbSe is able to reproduce the stability of the polymorphs with reasonably good agreement with the DFT results. The calculated RS-to-CsCl transition pressures for PbS and PbSe (Figure 2) are 14.5 and 15.6 GPa, respectively, which are in line with experimental measurements of 21.5 and 16 GPa for PbS and PbSe, respectively.[69]

We further test our transferable force field by reproducing the phonon dispersion relations of WZ-, ZB-CdX, and RS-PbX. These vibration properties were not used in the fitting procedures. Figures 3(a)–3(d) show the calculated phonon dispersion relations for WZ-CdS, WZ-CdSe, ZB-CdS, and ZB-CdSe, respectively. The paths in reciprocal space were chose as Γ → A for the WZ phase and Γ → L for the ZB phase. For WZ-CdX, the calculated phonon dispersion curves are in excellent agreement with the inelastic neutron scattering data[79,83] and DFT computations.[79,80] For ZB-CdX, there are no experimental data available for comparison. Only DFT-calculated phonon dispersion relations[81] and a few frequencies at the high symmetrical points estimated from the WZ-CdX measurements[5] can be used for comparison. In general, the phonon dispersion relations calculated for ZB-CdX using this force field are in agreement with the DFT calculations. Figures 3(e) and 3(f) show the calculated phonon dispersion curves in the direction of Γ → L for RS-PbS and RS-PbSe, respectively. Unlike the CdX, the calculated phonon curves for PbX deviate from the experimental data[84] and DFT calculations,[82] especially for the optical modes. Accurately reproducing the phonon dispersions for lead chalcogenides is extremely difficult for the existing classical force fields. For example, the phonon dispersions of RS-PbSe are also calculated by the LJ model for PbSe[59] (red dotted lines in Figure 3(f)). Neither the present force field nor the LJ model[59] is able to accurately reproduce the optical branch of phonons in PbSe. The same issue is also present for the force fields developed of PbTe.[34,60] In the fitting procedures, we also attempted to include the frequencies of the optical modes at the Γ point to the training set within this pair potential model to improve the description of the phonon relations. No significantly improved result was found. We suspect that only using two-body interactions is insufficient to accurately describe the vibrations of the atoms in lead chalcogenides.

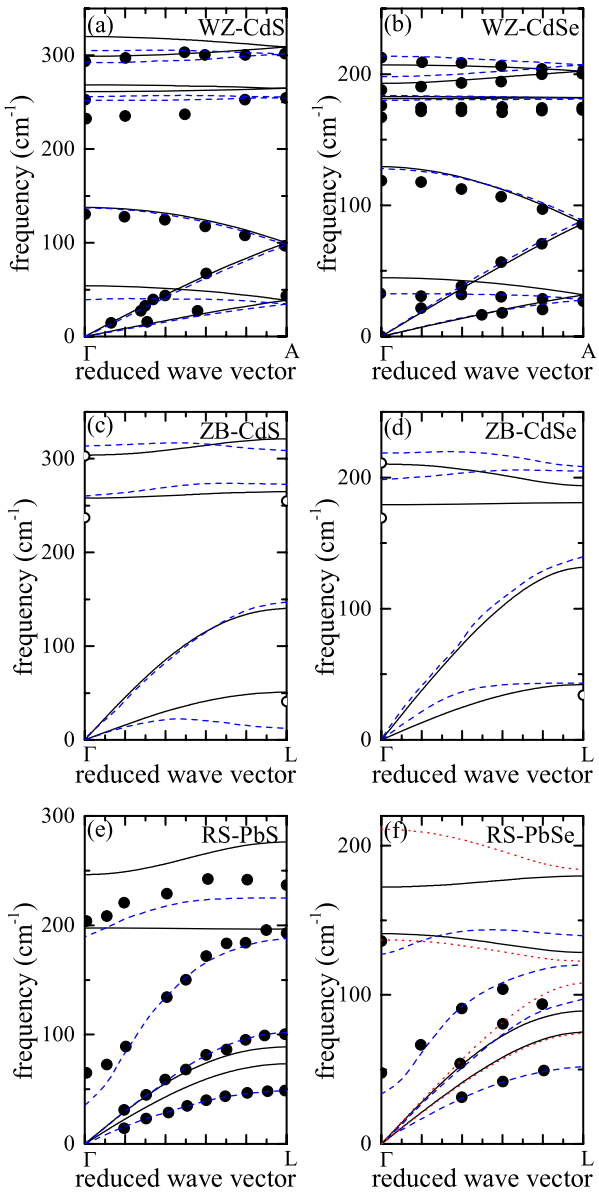

FIG. 3. Phonon dispersion relations of (a) WZ-CdS, (b) WZ-CdSe, (c) ZB-CdS, (d) ZB-CdSe, (e) RS-PbS, and (f) RS-PbSe. The paths in reciprocal space were chosen as Γ(0, 0, 0) → A(0, 0, 0.5) for the WZ phase and Γ(0, 0, 0) → L(0.5, 0.5, 0.5) for the ZB and RS phases. The black solid lines are the phonon dispersion curves calculated using this force field; the blue dashed lines are DFT calculations reported in Refs. 79–82; the circles are experimental data reported in Refs. 79 and 82–84; the diamonds are frequencies estimated from the experimental data of WZ-CdX;[5] and the red dotted lines are calculated using the LJ model for PbSe reported in Ref. 59.

IV. PHYSICAL PROPERTIES OF MIXED PHASES

So far, we have demonstrated that the new transferable force field is able to accurately reproduce several physical properties of CdS, CdSe, PbS, and PbSe binary compounds.

We expect that this transferable force field will also describe well mixed phases of these four binary compounds. We emphasize that three assumptions were made for the transferability in this model: (1) the same absolute value of the effective charge was used for all ions; (2) short-range interatomic interactions between cations were ignored; (3) the same parameters of short-range interatomic interactions between anions were used for different materials. The parameters for the cross term (short-range S-Se interaction) were obtained by fitting to DFT-calculated lattice parameters and stabilities of different QMPs. If these assumptions are reasonable, we should be able to use this force field to compute some basic physical properties of the mixed phases that are in agreement with the experimental and DFT data.

Table VI lists the lattice parameters and relative stabilities of different QMPs (WZ'-, ZB'-, RS'-Cd_2SSe and RS'-, ZB'-, and HC'-Pb_2SSe) calculated by this force field. A comparison is made with the values calculated by DFT and the LJ model of Ref. 39 (only available for Cd_2SSe). Note that in the LJ model,[39] the Lorentz-Berthelot mixing rules were used to obtain the parameters for all cross terms. Since the DFT data were used in the training set to obtain the parameters of the cross terms, our force field is able to more accurately reproduce the DFT results in comparison to the LJ model.[39]

In the general case, the cations or anions in mixed phases are more randomly distributed than in the QMPs in our DFT calculations. The chalcogenides with the same cation have the same crystal structure and similar lattice parameters. Therefore, their mixed phase forms continuous solid solution within a wide temperature range.[85,86] MD simulations were used to reproduce the lattice parameters of WZ-$CdS_{1-x}Se_x$ and RS-$PbS_{1-x}Se_x$ with different values of x from 0 to1. In the MD simulations, the WZ-CdS and RS-PbS matrixes were used as the initial configurations, and in each MD simulation 1/16 of the total number of S were randomly selected and replaced with Se. Thus the rate at which the ions were exchanged was approximately 30 anions per 500 ps. As expected, WZ-$CdS_{1-x}Se_x$ and RS-$PbS_{1-x}Se_x$ mixed phases formed solid solutions within the range of x from 0 to 1. $CdS_{1-x}Se_x$ remained WZ while $PbS_{1-x}Se_x$ remained RS. No phase transition or (local) structural distortion was found in the simulations. Figure 4 shows the relative lattice parameters of WZ-$CdS_{1-x}Se_x$ and RS-$PbS_{1-x}Se_x$ as function of x, which are in good agreement with experimental results.[85,86]

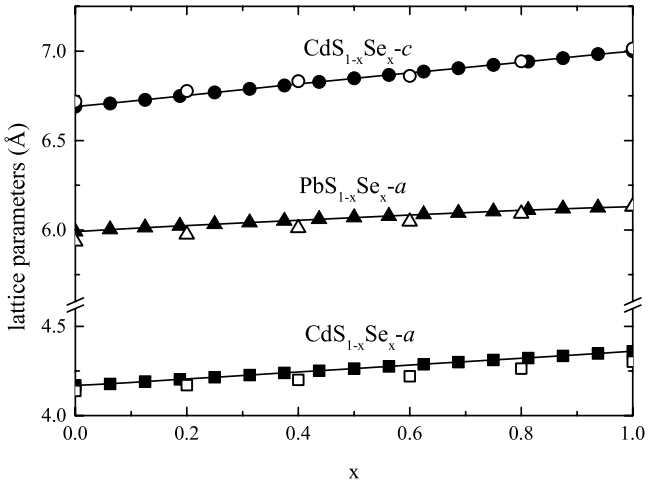

FIG. 4. Lattice parameters of $CdS_{1-x}Se_x$ and $PbS_{1-x}Se_x$ calculated from the MD simulations as a function of the fraction x using our new force field. The circles and the squares are the lattice parameter c and a in WZ-$CdS_{1-x}Se_x$, respectively; the triangles are the lattice parameter c in RS-$PbS_{1-x}Se_x$. The solid symbols are from the MD simulations and the open symbols are experimental measurements reported in Refs. 85 and 86.

In contradiction to the chalcogenides with the same cations, those with the same anions but different cations have different crystal structures. A six-fold ↔ four-fold phase transition should be observed in WZ-$Pb_xCd_{1-x}X$ (x: 0 → 1) and RS-$Pb_xCd_{1-x}X$ (x: 1 → 0) with increased/decreased fraction of Pb. This two-way phase transitions are difficult to be directly observed in bulk materials but have been observed in heteronanostructures that were initiated by cation exchange.[30,32] For this type of mixed phases, no additional parameter is needed for the force field. The transferability of the force field for describing the interatomic interactions between Cd and Pb is based on the assumption that the interatomic interactions between cations are only Coulomb interactions. We first compare

TABLE VI. Lattice parameters and relative stabilities of Cd_2SSe and Pb_2SSe quasi-mixed phases (QMPs) calculated using the present force field and the LJ models of Ref. 39, in comparison with DFT data. The lattice parameters a and c are in Å; the relative energy difference ΔE is in eV/f.u. The number 0 indicates the most stable phase among different structures. The lattice parameters from DFT calculations are normalized by rescaling their volumes. The values in bold are data used for the fit of the force field parameters.

	RS'[a]			ZB'[a]			WZ'[a] or HC'[a]		
	a	c	ΔE	a	c	ΔE	a	c	ΔE
Cd_2SSe									
DFT, this work	**5.52**	**5.52**	**0.298**	**5.95**	**5.96**	**0**	**4.21**	**6.88**	**0.004**
PCRIM, this work	5.53	5.54	0.299	5.94	5.94	0.005	4.22	6.81	0
LJ model[b]	5.61	5.57	0.134	6.00	5.96	0.018	4.28	6.78	0
Pb_2SSe									
DFT, this work	**6.04**	**6.04**	**0**	**6.69**	**6.68**	**0.354**	**5.06**	**6.05**	**0.158**
PCRIM, this work	6.02	6.02	0	6.79	6.69	0.363	5.13	5.99	0.193

[a]The prime symbols on the abbreviations of the structures denote the distortion and the reduced symmetry of the structures by replacing S with Se. See text and Figure 1.
[b]Calculated using the LJ model reported in Ref. 39.

the zero-temperature results by lattice statics simulations to available DFT data.[30] In the lattice statics simulations, 3×3×2 (72 atoms) and 2×2×2 (64 atoms) superlattices were constructed for WZ-CdSe and RS-PbSe as initial configurations, respectively. For each simulation, 4 randomly selected cations (either Cd in WZ-CdSe or Pb in RS-PbSe) were replaced by the other type of cations and a full geometrical relaxation was preformed for the superlattice. A simulation continued until all cations in a superlattice were replaced by the other type. Therefore, the lattice energies of the WZ- or RS-$Pb_xCd_{1-x}Se$ mixed phases with different fractions of x can be obtained. At zero temperature and zero pressure conditions, the Gibbs Free energy equals the lattice energy, $G = E$. Therefore, the relative energy difference for a particular fraction of Pb can be calculated as[30]

$$\Delta E_{Pb_xCd_{1-x}Se} = E_{Pb_xCd_{1-x}Se} - xE^{RS}_{PbSe} - (1-x)E^{WZ}_{CdSe}, \quad (2)$$

where E^{RS}_{PbSe} and E^{WZ}_{CdSe} are the lattice energies of RS-PbSe or WZ-CdSe. The calculated relative energy differences for WZ-$Pb_xCd_{1-x}Se$ (x: 0 → 1) and RS-$Pb_xCd_{1-x}Se$ (x: 1 → 0) are shown in Figure 5. The values calculated by the force field are in reasonable agreement with the available DFT data.[30] Both calculations predict an automatic WZ-to-HC structural transition in WZ-$Pb_xCd_{1-x}Se$ with increasing fraction of Pb. This structural transition only took place when x → 1 according to DFT calculations, but is found to be a gradual transition in the range of x = 0.6 ~ 1 using the force field. The calculated relative energy differences at 0 K are all positive indicating a complete phase separation of PbSe and CdSe.

To reproduce the concentration-induced six-fold ↔ four-fold phase transition in the $Pb_xCd_{1-x}X$ mixed phases, four independent MD simulations were carried out: WZ-$Pb_xCd_{1-x}X$ with x = 0 → 1 and RS-$Pb_xCd_{1-x}X$ with x = 1 → 0. The method mentioned earlier in the text was used to replace cations. The rate at which the ions were exchanged was also kept at ~30 cations per 500 ps. This exchange rate is larger than in experiments[30] (typically a few minutes for a complete cation exchange of a 20 nm-sized NC), but it is slow enough to observe phase transitions in the MD simulations. Apparently, using this artificial cation exchange, the MD simulations by no means are able to reveal the mechanisms of the real cation exchange phenomenon. We here only show the occurrences, possible routes, and mechanisms of these phase transitions initiated by cation exchange. We used a relatively high temperature (T = 500 K) for these MD simulations. The DFT computations of the relative stability of the ternary systems at zero temperature and a rough estimation considering the configurational entropy indicated that at relatively low temperatures ($T \leq 300$ K), a mixed phase is thermodynamically not favored over phase separation. A relatively high temperature is required to enable the $Pb_xCd_{1-x}X$ ternary systems to form mixed phases. A high temperature also provides the activation energy to cross energy barriers and therefore the phase transitions can be easily detected within a relatively short MD simulation time. Figure 6 shows typical snapshots of the four MD simulations at the transition concentrations. A WZ-to-RS phase transition (Figure 6(a)) was found as expected in the WZ-$Pb_xCd_{1-x}S$ system at x = 1/2, but, unexpectedly, the WZ-$Pb_xCd_{1-x}Se$ was trapped in a metastable HC phase (Figure 6(b) from x = 3/8 ~ 1). We feel that a higher temperature or a longer simulation time may enable the $Pb_xCd_{1-x}Se$ ($x \geq 0.5$) mixed phase to leap from the metastable HC phase to the stable RS phase, since such transformation involves activated nucleation events.[57] Surprisingly, the MD simulations starting from RS-$Pb_xCd_{1-x}S$ and RS-$Pb_xCd_{1-x}Se$ (x: 1 → 0) also yielded different results. The RS-$Pb_xCd_{1-x}Se$ mixed phase transform to the WZ structure at x = 3/4 (Figure 6(c)), while the RS-$Pb_xCd_{1-x}S$ mixed phase transform to the ZB structures from x=1/2 (Figure 6(d)). However, both results are acceptable since the WZ and ZB phases for CdX have very similar stabilities and the transition routes are expected to be highly sensitive to the temperature, the initial configuration, nucleation energies, energy barriers to transform from one phase to another, the rate at which the cations are exchanged, etc. Very recently, it was reported that both the RS-to-ZB and partially RS-to-WZ transitions are found by a cation exchange (Pb → Cd) process in RS-PbSe 2D-superlattices.[32]

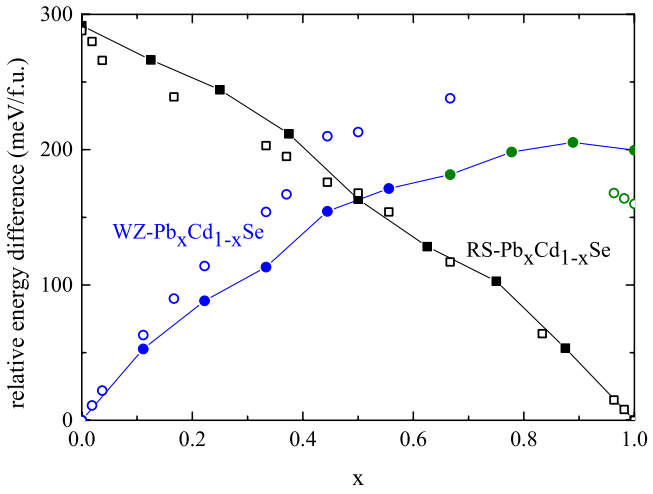

FIG. 5. Relative energy difference for the WZ- and RS-$Pb_xCd_{1-x}Se$ mixed phases as a function of x at 0 K. The circles are WZ-$Pb_xCd_{1-x}Se$ with increasing x from 0 to 1; the squares are RS-$Pb_xCd_{1-x}Se$ with decreasing x from 1 to 0. The solid symbols are calculated using the force field and the open symbols are DFT data reported in Ref. 30. The colors black, blue, and green indicate the RS, WZ, and HC structures, respectively.

V. SURFACE ENERGY CALCULATIONS

Using this force field, the surface energies of several different non-polar surfaces of WZ-CdX and RS-PbX were calculated and were compared with the results calculated by the LJ models[39,55,59] and by DFT. For the WZ-CdX, the $\{10\bar{1}0\}$ and $\{11\bar{2}0\}$ surfaces were considered while for RS-PbX, the {100} and {110} surfaces were considered. These non-polar surfaces are the most important surfaces for WZ-CdX and RS-PbX having the lowest surface energies. Polar surfaces as WZ-±{0001} and RS-±{111} are also important, but the stabilizing mechanisms are complicated and can differ between different materials or between different terminated atoms (i.e., cation-terminated, anion-terminated, or reconstructed polar surfaces).[33,38,87–89] Surface energies of those polar surfaces calculated by DFT and by classical force fields

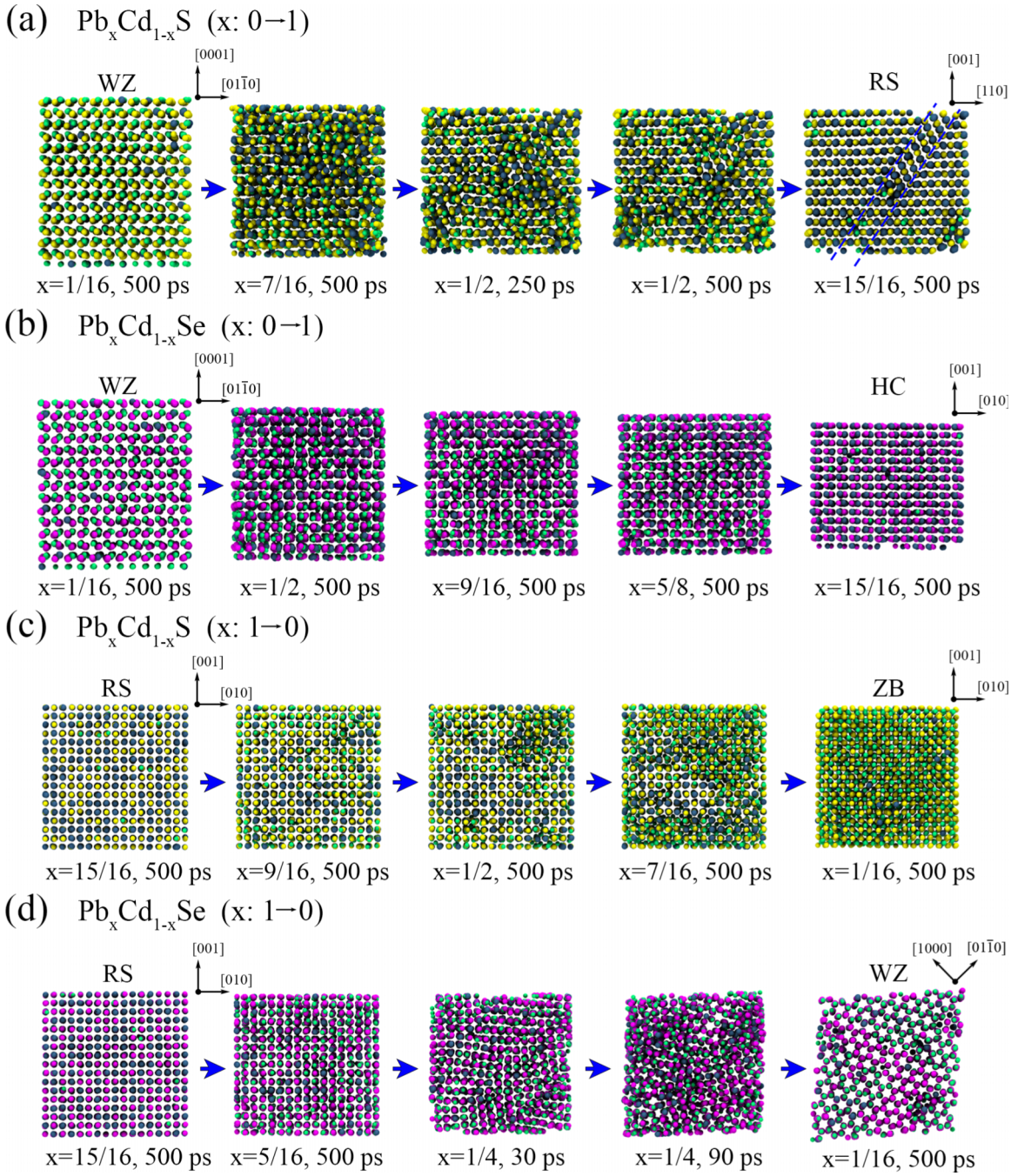

FIG. 6. Snapshots of MD simulations of (a) WZ-Pb$_x$Cd$_{1-x}$S (x: 0 → 1), (b) WZ-Pb$_x$Cd$_{1-x}$Se (x: 0 → 1), (c) RS-Pb$_x$Cd$_{1-x}$S (x: 1 → 0), and (d) RS-Pb$_x$Cd$_{1-x}$Se (x: 1 → 0) ternary mixed phases at 500 K. The green, blue, yellow, and purple spheres represent Cd, Pb, S, and Se atoms, respectively. For each system, the first and the last snapshots show the final configurations with the lowest and highest fractions of exchanged cations, respectively; the second to the fourth snapshots show the configurations when the phase transitions are taking place. The blue dashed lines at the upper right of the figure indicate twin boundaries in the RS-Pb$_{15/16}$Cd$_{1/16}$S.

are normally of the same order of magnitude.[33,40] However, DFT and classical force fields in general use very different schemes to calculate polar surfaces,[33] thus the comparison between them is difficult and less meaningful. Therefore, we omit the calculations and discussions of the polar surfaces. For the details about the DFT and classical computations of surface energy, we refer to our previous work.[33]

Table VII shows the calculated surface energies by the present PCRIM, the LJ models,[39,55,59] and DFT for CdX and PbX, respectively. We expect that the materials with the same cations have similar surface properties, since they have the same structures and the very similar physical properties. However, the DFT results for CdSe reported by Manna *et al.*[88] and Csik *et al.*[90] are very different from those for CdS reported by Barnard *et al.*[87] The former are almost two times larger than the latter. The authors from the last paper suggested that the difference may be due to the different schemes used in the DFT calculations and/or the different materials studied. We performed the DFT-GGA calculations for both CdS and CdSe. It turns out that our results for CdS are similar to those

TABLE VII. Surface energies of the most stable non-polar surfaces for CdX and PbX calculated with the present force field, the LJ models of Refs. 39 and 59, and by DFT, together with available DFT data in literature. The surface energies are in J/m^2.

	Surface	PCRIM, this work	LJ model[a]	DFT, this work	DFT, literature
WZ-CdS	$\{10\bar{1}0\}$	0.29	0.42	0.323	0.28[b]
	$\{11\bar{2}0\}$	0.30	0.44	0.318	0.29[b]
WZ-CdSe	$\{10\bar{1}0\}$	0.25	0.35	0.237	0.46[c], 0.59[d]
	$\{11\bar{2}0\}$	0.26	0.37	0.231	0.50[c], 0.67[d]
RS-PbS	{100}	0.29	...	0.178	0.160[e]
	{110}	0.49	...	0.327	...
RS-PbSe	{100}	0.29	0.33	0.179	0.184[f]
	{110}	0.49	0.67	0.316	0.318[f]

[a]Calculated using the LJ models reported in Refs. 39 and 59.
[b]Reference 87.
[c]Reference 90.
[d]Reference 88.
[e]Reference 89.
[f]Reference 38.

reported in Ref. 87 and the values for CdSe are slightly smaller than those for CdS. In our DFT calculations, we used the same basic settings with considerably high accuracy for all materials, which indicates that the surface properties for CdS and CdSe are indeed similar and these significant differences from former DFT calculations are likely due to the different computational methods used. Similarity is also found between the surfaces of PbS[89] and PbSe.[38] The surface energies for CdX and PbX calculated by our force field are in reasonable agreement with our DFT calculations. The calculated surface energies of the {001} facet of PbX (~0.29 J/m^2) are slightly higher than the DFT results (~0.18 J/m^2). For WZ-CdX, the two most stable surfaces, $\{10\bar{1}0\}$ and $\{11\bar{2}0\}$, have very similar surface energies, which dominate the morphologies of the WZ-CdX nanostructures (e.g., WZ-CdX NCs normally form spheres and rods). For RS-PbX, the {100} facet has the lowest surface energy, thus PbX NCs easily form cubes or truncated cubes.

VI. CONCLUSIONS

We have significantly extended our previously published transferable force field for the CdSe-PbSe systems[30] to the CdS-CdSe-PbS-PbSe systems. This partially charged rigid ion model contains only two-body interatomic interactions and 22 parameters. This new force field has simple functional forms but equivalent or better descriptions of several physical properties of CdX and PbX in comparison to other models. The physical properties of CdX and PbX including the crystalline structures, elastic constants, bulk moduli, relative stability, transition pressures, phonon dispersion relations, and the surface energy can be described by this force field with considerably high accuracy. This force field is also able to describe the MS_xSe_{1-x} and $Cd_xPb_{1-x}X$ ternary systems. The former forms continuous solid solutions while concentration-induced four-fold (WZ or ZB) ↔ six-fold (RS) transitions were found in the latter by changing the fraction of the cations. We also summarize the shortcomings for this force field: (1) according to our DFT-GGA calculations, the stability of the HC phase is slightly overestimated and that of the ZB phase is slightly underestimated for CdX. (2) Due to the simplification of this PCRIM, several physical properties cannot be accurately reproduced for CdX and/or PbX, including the cohesive energies and melting points for CdX and PbX, and the phonons in RS-PbX. The melting points of WZ-CdS, WZ-CdSe, RS-PbS, and RS-PbSe assessed by direct heating MD simulations[33] are 1137, 1088, 1665, and 1608 K, respectively. The experimentally measured melting points[5,7] are 1748, 1512, 1383, and 1353 K for WZ-CdS, WZ-CdSe, RS-PbS, and RS-PbSe, respectively. Note that the force field was not tuned to reproduce experimental melting points. (3) The calculated surface energies of the {100} facet of PbX are slightly higher than the DFT results. The charge transfer on the polar surfaces of the CdX and PbX cannot be described by the rigid ion model.

A classical force field can never perfectly describe the quantum world. However, using suitable functional forms with careful parameterization, a derived classical force field with simple functional forms can capture many essential physical and chemical properties of materials and is useful in the atomistic simulations for large systems (e.g., nanostructures). Many unsolved problems or burgeoning research in material science such as solid-solid phase transitions, the seeded growth mechanism, oriented attachment, and cation exchange of NCs are expected to be studied in depth at atomic level with the aid of classical molecular simulations, which are of interest for the further development of functional chalcogenide nanostructures.

ACKNOWLEDGMENTS

This work is part of the research program of the Foundation for Fundamental Research on Matter (FOM), which is part of the Netherlands Organisation for Scientific Research (NWO). This work was also sponsored by the Stichting Nationale Computerfaciliteiten (National Computing Facilities Foundation, NCF, Grant No. MP-213-14) for the use of supercomputing facilities, with financial support from NWO. M.v.H. acknowledges NWO for a VIDI grant (Grant No. 723.012.006).

[1]X. Peng, L. Manna, W. Yang, J. Wickham, E. Scher, A. Kadavanich, and A. P. Alivisatos, "Shape control of CdSe nanocrystals," Nature **404**, 59–61 (2000).

[2]Z. A. Peng and X. Peng, "Formation of high-quality CdTe, CdSe, and CdS nanocrystals using CdO as precursor," J. Am. Chem. Soc. **123**, 183–184 (2001).
[3]R. D. Schaller and V. I. Klimov, "High efficiency carrier multiplication in PbSe nanocrystals: Implications for solar energy conversion," Phys. Rev. Lett. **92**, 186601 (2004).
[4]R. J. Ellingson, M. C. Beard, J. C. Johnson, P. Yu, O. I. Micic, A. J. Nozik, A. Shabaev, and A. L. Efros, "Highly efficient multiple exciton generation in colloidal PbSe and PbS quantum dots," Nano Lett. **5**, 865–871 (2005).
[5]A. Sadao, *Properties of Group-IV, III-V and II-VI Semiconductors* (Wiley, New York, 2005).
[6]A. P. Alivisatos, "Semiconductor clusters, nanocrystals, and quantum dots," Science **271**, 933–937 (1996).
[7]O. Madelung, U. Rössler, and M. Schulz, *Landolt-Börnstein III/41C: Non-Tetrahedrally Bonded Elements and Binary Compounds I* (Springer-Verlag, Berlin, Germany, 1998).
[8]M. Fardy, A. I. Hochbaum, J. Goldberger, M. M. Zhang, and P. Yang, "Synthesis and thermoelectrical characterization of lead chalcogenide nanowires," Adv. Mater. **19**, 3047–3051 (2007).
[9]R. Y. Wang, J. P. Feser, J.-S. Lee, D. V. Talapin, R. Segalman, and A. Majumdar, "Enhanced thermopower in PbSe nanocrystal quantum dot superlattices," Nano Lett. **8**, 2283–2288 (2008).
[10]K.-T. Yong, Y. Sahoo, M. T. Swihart, and P. N. Prasad, "Shape control of CdS nanocrystals in one-pot synthesis," J. Phys. Chem. C **111**, 2447–2458 (2007).
[11]K. P. Rice, A. E. Saunders, and M. P. Stoykovich, "Seed-mediated growth of shape-controlled wurtzite CdSe nanocrystals: Platelets, cubes, and rods," J. Am. Chem. Soc. **135**, 6669–6676 (2013).
[12]W. W. Yu, Y. A. Wang, and X. Peng, "Formation and stability of size-, shape-, and structure-controlled CdTe nanocrystals: A ligand effects on monomers and nanocrystals," Chem. Mater. **15**, 4300–4308 (2003).
[13]G. Zhou, M. Lu, Z. Xiu, S. Wang, H. Zhang, Y. Zhou, and S. Wang, "Controlled synthesis of high-quality PbS star-shaped dendrites, multipods, truncated nanocubes, and nanocubes and their shape evolution process," J. Phys. Chem. B **110**, 6543–6548 (2006).
[14]E. Lifshitz, M. Bashouti, V. Kloper, A. Kigel, M. S. Eisen, and S. Berger, "Synthesis and characterization of PbSe quantum wires, multipods, quantum rods, and cubes," Nano Lett. **3**, 857–862 (2003).
[15]T. Mokari, M. Zhang, and P. Yang, "Shape, size, and assembly control of PbTe nanocrystals," J. Am. Chem. Soc. **129**, 9864–9865 (2007).
[16]D. V. Talapin, R. Koeppe, S. Gotzinger, A. Kornowski, J. M. Lupton, A. L. Rogach, O. Benson, J. Feldmann, and H. Weller, "Highly emissive colloidal CdSe/CdS heterostructures of mixed dimensionality," Nano Lett. **3**, 1677–1681 (2003).
[17]D. J. Milliron, S. M. Hughes, Y. Cui, L. Manna, J. Li, L.-W. Wang, and A. P. Alivisatos, "Colloidal nanocrystal heterostructures with linear and branched topology," Nature **430**, 190–195 (2004).
[18]S. Deka, K. Miszta, D. Dorfs, A. Genovese, G. Bertoni, and L. Manna, "Octapod-shaped colloidal nanocrystals of cadmium chalcogenides via "one-pot" cation exchange and seeded growth," Nano Lett. **10**, 3770–3776 (2010).
[19]S. Kudera, L. Carbone, M. F. Casula, R. Cingolani, A. Falqui, E. Snoeck, W. J. Parak, and L. Manna, "Selective growth of PbSe on one or both tips of colloidal semiconductor nanorods," Nano Lett. **5**, 445–449 (2005).
[20]W. Lv, W. He, X. Wang, Y. Niu, H. Cao, J. H. Dickerson, and Z. Wang, "Understanding the oriented-attachment growth of nanocrystals from an energy point of view: A review," Nanoscale **6**, 2531–2547 (2014).
[21]S. Gupta, S. V. Kershaw, and A. L. Rogach, "25th anniversary article: Ion exchange in colloidal nanocrystals," Adv. Mater. **25**, 6923–6944 (2013).
[22]J. B. Rivest and P. K. Jain, "Cation exchange on the nanoscale: An emerging technique for new material synthesis, device fabrication, and chemical sensing," Chem. Soc. Rev. **42**, 89–96 (2013).
[23]R. L. Penn and J. F. Banfield, "Imperfect oriented attachment: Dislocation generation in defect-free nanocrystals," Science **281**, 969–971 (1998).
[24]K.-S. Cho, D. V. Talapin, W. Gaschler, and C. B. Murray, "Designing PbSe nanowires and nanorings through oriented attachment of nanoparticles," J. Am. Chem. Soc. **127**, 7140–7147 (2005).
[25]C. Schliehe, B. H. Juarez, M. Pelletier, S. Jander, D. Greshnykh, M. Nagel, A. Meyer, S. Foerster, A. Kornowski, C. Klinke, and H. Weller, "Ultrathin PbS sheets by two-dimensional oriented attachment," Science **329**, 550–553 (2010).
[26]G. Jia, A. Sitt, G. B. Hitin, I. Hadar, Y. Bekenstein, Y. Amit, I. Popov, and U. Banin, "Couples of colloidal semiconductor nanorods formed by self-limited assembly," Nat. Mater. **13**, 301–307 (2014).
[27]D. H. Son, S. M. Hughes, Y. Yin, and A. P. Alivisatos, "Cation exchange reactions in ionic nanocrystals," Science **306**, 1009–1012 (2004).
[28]M. Casavola, M. A. van Huis, S. Bals, K. Lambert, Z. Hens, and D. Vanmaekelbergh, "Anisotropic cation exchange in PbSe/CdSe core/shell nanocrystals of different geometry," Chem. Mater. **24**, 294–302 (2011).
[29]J. M. Luther, H. Zheng, B. Sadtler, and A. P. Alivisatos, "Synthesis of PbS nanorods and other ionic nanocrystals of complex morphology by sequential cation exchange reactions," J. Am. Chem. Soc. **131**, 16851–16857 (2009).
[30]A. O. Yalcin, Z. Fan, B. Goris, W.-F. Li, R. S. Koster, C.-M. Fang, A. van Blaaderen, M. Casavola, F. D. Tichelaar, S. Bals, G. Van Tendeloo, T. J. H. Vlugt, D. Vanmaekelbergh, H. W. Zandbergen, and M. A. van Huis, "Atomic resolution monitoring of cation exchange in CdSe-PbSe heteronanocrystals during epitaxial solid-solid-vapor growth," Nano Lett. **14**, 3661–3667 (2014).
[31]M. Saruyama, Y.-G. So, K. Kimoto, S. Taguchi, Y. Kanemitsu, and T. Teranishi, "Spontaneous formation of wurzite-CdS/zinc blende-CdTe heterodimers through a partial anion exchange reaction," J. Am. Chem. Soc. **133**, 17598–17601 (2011).
[32]M. P. Boneschanscher, W. H. Evers, J. J. Geuchies, T. Altantzis, B. Goris, F. T. Rabouw, S. A. P. van Rossum, H. S. J. van der Zant, L. D. A. Siebbeles, G. van Tendeloo, I. Swart, J. Hilhorst, A. V. Petukhov, S. Bals, and D. Vanmaekelbergh, "Long-range orientation and atomic attachment of nanocrystals in 2d honeycomb superlattices," Science **344**, 1377–1380 (2014).
[33]S. Wang, Z. Fan, R. S. Koster, C. Fang, M. A. van Huis, A. O. Yalcin, F. D. Tichelaar, H. W. Zandbergen, and T. J. H. Vlugt, "New ab initio based pair potential for accurate simulation of phase transitions in ZnO," J. Phys. Chem. C **118**, 11050–11061 (2014).
[34]H. Kim and M. Kaviany, "Effect of thermal disorder on high figure of merit in PbTe," Phys. Rev. B **86**, 045213 (2012).
[35]K. Sarasamak, A. J. Kulkarni, M. Zhou, and S. Limpijumnong, "Stability of wurtzite, unbuckled wurtzite, and rocksalt phases of SiC, GaN, InN, ZnO, and CdSe under loading of different triaxialities," Phys. Rev. B **77**, 024104 (2008).
[36]J. Cai and N. Chen, "First-principles study of the wurtzite-to-rocksalt phase transition in zinc oxide," J. Phys.: Condens. Matter **19**, 266207 (2007).
[37]S. Limpijumnong and S. Jungthawan, "First-principles study of the wurtzite-to-rocksalt homogeneous transformation in ZnO: A case of a low-transformation barrier," Phys. Rev. B **70**, 054104 (2004).
[38]C. Fang, M. A. van Huis, D. Vanmaekelbergh, and H. W. Zandbergen, "Energetics of polar and nonpolar facets of PbSe nanocrystals from theory and experiment," ACS Nano **4**, 211–218 (2010).
[39]M. Grünwald, A. Zayak, J. B. Neaton, P. L. Geissler, and E. Rabani, "Transferable pair potentials for CdS and ZnS crystals," J. Chem. Phys. **136**, 234111 (2012).
[40]Z. Fan, A. O. Yalcin, F. D. Tichelaar, H. W. Zandbergen, E. Talgorn, A. J. Houtepen, T. J. H. Vlugt, and M. A. van Huis, "From sphere to multipod: Thermally induced transitions of CdSe nanocrystals studied by molecular dynamics simulations," J. Am. Chem. Soc. **135**, 5869–5876 (2013).
[41]R. Agrawal, B. Peng, and H. D. Espinosa, "Experimental-computational investigation of ZnO nanowires strength and fracture," Nano Lett. **9**, 4177–4183 (2009).
[42]K. Wright and J. D. Gale, "Interatomic potentials for the simulation of the zinc-blende and wurtzite forms of ZnS and CdS: Bulk structure, properties, and phase stability," Phys. Rev. B **70**, 035211 (2004).
[43]B. G. Dick and A. W. Overhauser, "Theory of the dielectric constants of alkali halide crystals," Phys. Rev. **112**, 90–103 (1958).
[44]J. C. Phillips, "Covalent bond in crystals. I. Elements of a structural theory," Phys. Rev. **166**, 832–838 (1968).
[45]C. R. A. Catlow and A. M. Stoneham, "Ionicity in solids," J. Phys. C: Solid State Phys. **16**, 4321 (1983).
[46]C. R. A. Catlow and W. C. Mackrodt, "Computer simulation of solids," *Lecture Notes in Physics* (Springer-Verlag, Berlin, 1982), Vol. 166.
[47]C. R. A. Catlow, S. A. French, A. A. Sokol, A. A. Al-Sunaidi, and S. M. Woodley, "Zinc oxide: A case study in contemporary computational solid state chemistry," J. Comput. Chem. **29**, 2234–2249 (2008).
[48]G. V. Lewis and C. R. A. Catlow, "Potential models for ionic oxides," J. Phys. C: Solid State Phys. **18**, 1149 (1985).
[49]B. W. H. van Beest, G. J. Kramer, and R. A. van Santen, "Force fields for silicas and aluminophosphates based on *ab initio* calculations," Phys. Rev. Lett. **64**, 1955–1958 (1990).

[50]D. J. Binks and R. W. Grimes, "Incorporation of monovalent ions in ZnO and their influence on varistor degradation," J. Am. Ceram. Soc. **76**, 2370–2372 (1993).
[51]M. J. Sanders, M. Leslie, and C. R. A. Catlow, "Interatomic potentials for SiO_2," J. Chem. Soc., Chem. Commun. **1984**, 1271–1273
[52]X. W. Zhou, D. K. Ward, J. E. Martin, F. B. van Swol, J. L. Cruz-Campa, and D. Zubia, "Stillinger-weber potential for the II-VI elements Zn-Cd-Hg-S-Se-Te," Phys. Rev. B **88**, 085309 (2013).
[53]D. K. Ward, X. W. Zhou, B. M. Wong, F. P. Doty, and J. A. Zimmerman, "Analytical bond-order potential for the Cd-Zn-Te ternary system," Phys. Rev. B **86**, 245203 (2012).
[54]S. Tsuneyuki, M. Tsukada, H. Aoki, and Y. Matsui, "First-principles interatomic potential of silica applied to molecular dynamics," Phys. Rev. Lett. **61**, 869–872 (1988).
[55]E. Rabani, "An interatomic pair potential for cadmium selenide," J. Chem. Phys. **116**, 258–262 (2002).
[56]D. Zahn, Y. Grin, and S. Leoni, "Mechanism of the pressure-induced wurtzite to rocksalt transition of CdSe," Phys. Rev. B **72**, 064110 (2005).
[57]M. Grünwald, E. Rabani, and C. Dellago, "Mechanisms of the wurtzite to rocksalt transformation in CdSe nanocrystals," Phys. Rev. Lett. **96**, 255701 (2006).
[58]M. Grünwald, K. Lutker, A. P. Alivisatos, E. Rabani, and P. L. Geissler, "Metastability in pressure-induced structural transformations of CdSe/ZnS core/shell nanocrystals," Nano Lett. **13**, 1367–1372 (2012).
[59]P. Schapotschnikow, M. A. van Huis, H. W. Zandbergen, D. Vanmaekelbergh, and T. J. H. Vlugt, "Morphological transformations and fusion of PbSe nanocrystals studied using atomistic simulations," Nano Lett. **10**, 3966–3971 (2010).
[60]B. Qiu, H. Bao, G. Zhang, Y. Wu, and X. Ruan, "Molecular dynamics simulations of lattice thermal conductivity and spectral phonon mean free path of PbTe: Bulk and nanostructures," Comput. Mater. Sci. **53**, 278–285 (2012).
[61]J. D. Gale, "Empirical potential derivation for ionic materials," Philos. Mag. B **73**, 3–19 (1996).
[62]R. F. W. Bader, *Atoms in Molecules - A Quantum Theory* (Oxford University Press, Oxford, 1990).
[63]J. D. Gale and A. L. Rohl, "The general utility lattice program (gulp)," Mol. Simul. **29**, 291–341 (2003).
[64]P. P. Ewald, "Die berechnung optischer und elektrostatischer gitterpotentiale," Ann. Phys. **369**, 253–287 (1921).
[65]D. Frenkel and B. Smit, *Understanding Molecular Simulation*, 2nd ed. (Academic Press, New York, 2002).
[66]G. J. Martyna, D. J. Tobias, and M. L. Klein, "Constant pressure molecular dynamics algorithms," J. Comput. Phys. **101**, 4177–4189 (1994).
[67]Y. Li, X. Zhang, H. Li, X. Li, C. Lin, W. Xiao, and J. Liu, "High pressure-induced phase transitions in CdS up to 1 mbar," J. Appl. Phys. **113**, 083509 (2013).
[68]Y. Li, C. Lin, G. Li, J. Xu, X. Li, and J. Liu, "Structure determination of the high-pressure phase of CdSe," J. Appl. Phys. **115**, 223507 (2014).
[69]T. Chattopadhyay, H. G. von Schnering, W. A. Grosshans, and W. B. Holzapfel, "High pressure x-ray diffraction study on the structural phase transitions in PbS, PbSe and PbTe with synchrotron radiation," Physica B+C **139–140**, 356–360 (1986).
[70]A. Aresti, L. Garbato, and A. Rucci, "Some cohesive energy features of tetrahedral semiconductors," J. Phys. Chem. Solid **45**, 361–365 (1984).
[71]S. E. Boulfelfel and S. Leoni, "Competing intermediates in the pressure-induced wurtzite to rocksalt phase transition in ZnO," Phys. Rev. B **78**, 125204 (2008).
[72]M. Wilson and P. A. Madden, "Transformations between tetrahedrally and octahedrally coordinated crystals," J. Phys.: Condens. Matter **14**, 4629 (2002).
[73]F. Shimojo, S. Kodiyalam, I. Ebbsjö, R. K. Kalia, A. Nakano, and P. Vashishta, "Atomistic mechanisms for wurtzite-to-rocksalt structural transformation in cadmium selenide under pressure," Phys. Rev. B **70**, 184111 (2004).
[74]D. Spagnoli and J. D. Gale, "Atomistic theory and simulation of the morphology and structure of ionic nanoparticles," Nanoscale **4**, 1051–1067 (2012).
[75]P. Zapol, R. Pandey, and J. D. Gale, "An interatomic potential study of the properties of gallium nitride," J. Phys.: Condens. Matter **9**, 9517 (1997).
[76]S. Hamad, S. Cristol, and C. R. A. Catlow, "Surface structures and crystal morphology of ZnS: Computational study," J. Phys. Chem. B **106**, 11002–11008 (2002).
[77]R. Ahuja, "High pressure structural phase transitions in IV-VI semiconductors," Phys. Status Solidi B **235**, 341–347 (2003).
[78]S. V. Ovsyannikov, V. V. Shchennikov, A. Y. Manakov, A. Y. Likhacheva, Y. S. Ponosov, V. E. Mogilenskikh, A. P. Vokhmyanin, A. I. Ancharov, and E. P. Skipetrov, "Unusual b1-b2 transition in PbSe under high pressure: Evidence for two intermediate phases; transport, structural, and optical properties," Phys. Status Solidi B **246**, 615–621 (2009).
[79]A. Debernardi, N. M. Pyka, A. Göbel, T. Ruf, R. Lauck, S. Kramp, and M. Cardona, "Lattice dynamics of wurtzite CdS: Neutron scattering and *ab-initio* calculations," Solid State Commun. **103**, 297–301 (1997).
[80]M. Mohr and C. Thomsen, "Phonons in bulk CdSe and CdSe nanowires," Nanotechnology **20**, 115707 (2009).
[81]E. Deligoz, K. Colakoglu, and Y. Ciftci, "Elastic, electronic, and lattice dynamical properties of CdS, CdSe, and CdTe," Phys. B **373**, 124–130 (2006).
[82]O. Kilian, G. Allan, and L. Wirtz, "Near kohn anomalies in the phonon dispersion relations of lead chalcogenides," Phys. Rev. B **80**, 245208 (2009).
[83]F. Widulle, S. Kramp, N. M. Pyka, A. Göbel, T. Ruf, A. Debernardi, R. Lauck, and M. Cardona, "The phonon dispersion of wurtzite CdSe," Phys. B **263-264**, 448–451 (1999).
[84]M. M. Elcombe, "The crystal dynamics of lead sulphide," Proc. R. Soc. A **300**, 210–217 (1967).
[85]U. Hotje, C. Rose, and M. Binnewies, "Lattice constants and molar volume in the system ZnS, ZnSe, CdS, CdSe," Solid State Sci. **5**, 1259–1262 (2003).
[86]H. Liu and L. L. Y. Chang, "Phase relations in the system PbS-PbSe-PbTe," Mineral. Mag. **58**, 567–578 (1994).
[87]A. S. Barnard and H. Xu, "First principles and thermodynamic modeling of CdS surfaces and nanorods," J. Phys. Chem. C **111**, 18112–18117 (2007).
[88]L. Manna, L. Wang, R. Cingolani, and A. P. Alivisatos, "First-principles modeling of unpassivated and surfactant-passivated bulk facets of wurtzite CdSe: A model system for studying the anisotropic growth of CdSe nanocrystals," J. Phys. Chem. B **109**, 6183–6192 (2005).
[89]L. Zhang, Q. Song, and S. B. Zhang, "Exceptionally strong hydrogen bonds affect the surface energy of colloidal nanocrystals: Methylamine and water adsorption on PbS," Phys. Rev. Lett. **104**, 116101 (2010).
[90]I. Csik, S. P. Russo, and P. Mulvaney, "Density functional study of non-polar surfaces of wurtzite CdSe," Chem. Phys. Lett. **414**, 322–325 (2005).